Eur. Phys. J. C 14, 633–641 (2000)
Digital Object Identifier (DOI) 10.1007/s100520000386

THE EUROPEAN PHYSICAL JOURNAL C

Transverse mass spectra of strange and multi–strange particles in Pb–Pb collisions at 158 A GeV/c

The WA97 Collaboration

F. Antinori[6,10], H. Bakke[2], W. Beusch[6], I.J. Bloodworth[4], R. Caliandro[1], N. Carrer[10], D. Di Bari[1], S. Di Liberto[12], D. Elia[1], D. Evans[4], K. Fanebust[2], R.A. Fini[1], J. Ftáčnik[7], B. Ghidini[1], G. Grella[13], M. Gulino[5], H. Helstrup[3], A.K. Holme[9], D. Huss[8], A. Jacholkowski[1], G.T. Jones[4], J.B. Kinson[4], K. Knudson[6], I. Králik[7], V. Lenti[1], R. Lietava[7], R.A. Loconsole[1], G. Løvhøiden[9], V. Manzari[1], M.A. Mazzoni[12], F. Meddi[12], A. Michalon[14], M.E. Michalon-Mentzer[14], M. Morando[10], P.I. Norman[4], B. Pastirčák[7], E. Quercigh[6], D. Röhrich[2], G. Romano[13], K. Šafařík[6], L. Šándor[6,7], G. Segato[10], P. Staroba[11], M. Thompson[4], T.F. Thorsteinsen[2,†], G.D. Torrieri[4], T.S. Tveter[9], J. Urbán[7], O. Villalobos Baillie[4], T. Virgili[13], M.F. Votruba[4], P. Závada[11]

[1] Dipartimento I.A. di Fisica dell'Università e del Politecnico di Bari and Sezione INFN, Bari, Italy
[2] Fysisk institutt, Universitetet i Bergen, Bergen, Norway
[3] Høgskolen i Bergen, Bergen, Norway
[4] School of Physics and Astronomy, University of Birmingham, Birmingham, UK
[5] University of Catania and INFN, Catania, Italy
[6] CERN, European Laboratory for Particle Physics, Geneva, Switzerland
[7] Institute of Experimental Physics, Slovak Academy of Sciences, Košice, Slovakia
[8] GRPHE, Université de Haute Alsace, Mulhouse, France
[9] Fysisk institutt, Universitetet i Oslo, Oslo, Norway
[10] Dipartimento di Fisica dell'Università and Sezione INFN, Padua, Italy
[11] Institute of Physics, Academy of Sciences of Czech Republic, Prague, Czech Republic
[12] Dipartimento di Fisica dell'Università "La Sapienza" and Sezione INFN, Rome, Italy
[13] Dipartimento di Scienze Fisiche "E.R. Caianiello" dell'Università and INFN, Salerno, Italy
[14] Institut de Recherches Subatomiques, IN2P3/ULP, Strasbourg, France

Received: 5 January 2000 / Revised version: 28 February 2000 /
Published online: 14 April 2000 – © Springer-Verlag 2000

Abstract. The WA97 experiment has measured the transverse mass (m_{T}) spectra for negative hadrons (h^-) and strange particles produced at mid–rapidity in Pb–Pb collisions. The increased statistics of analysed data samples allowed us to perform a study of the spectra of $\mathrm{K}^0_{\mathrm{S}}$, Λ, Ξ, Ω and h^- as a function of the collision centrality. The data, which correspond to the most central 40% of the total inelastic cross section, have been divided into four centrality classes according to the estimated number of nucleons taking part in the collision. The m_{T} spectra, analysed separately for each centrality bin, exhibit only weak ($\leq 15\%$) centrality dependence. The deviation of the Ω inverse slope from the linear dependence on the particle mass is confirmed even for the most central Pb–Pb collisions.

1 Introduction

The systematic study of ultrarelativistic heavy ion collisions forms an important part of experimental activities at the BNL AGS and the CERN SPS. The investigation of properties of nuclear matter at extreme conditions is motivated mainly by the QCD prediction that at sufficiently high energy density the excited nuclear matter undergoes a phase transition into a system of deconfined quarks and gluons (Quark–Gluon Plasma - QGP). A number of experimental signatures which should signal the QGP have been proposed. For a recent review see e.g. [1,2].

Strange particles, produced in high-energy heavy-ion collisions, are expected to be a powerful tool for the study of reaction dynamics. In particular, the enhanced relative yield of strange and multi-strange particles and antiparticles in central nucleus-nucleus interactions, with respect to proton induced reactions, has been suggested as one of the signatures for a phase transition to a QGP state [3,4]. It is expected that the enhancement should be more pronounced for multi-strange than for singly-strange hadrons [5].

† Deceased

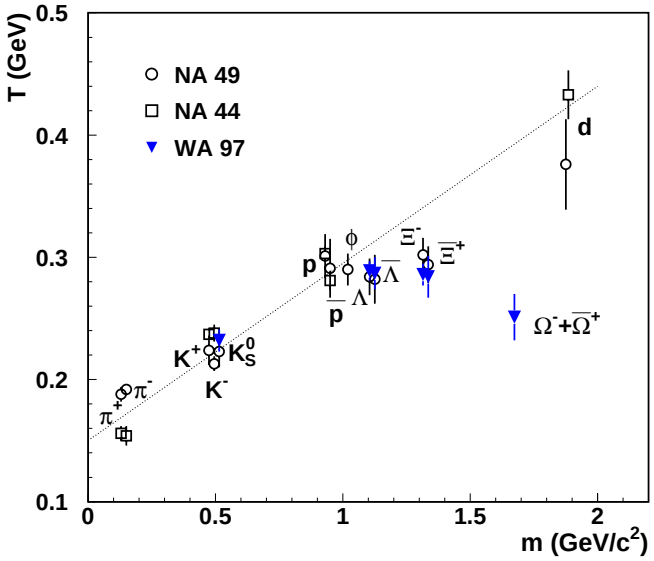

Fig. 1. Dependence of the m_{T} spectra inverse slopes T on the particle mass m for Pb–Pb collisions at SPS energy. The line represents an approximation of the RQMD model calculations for non-strange particles [18]

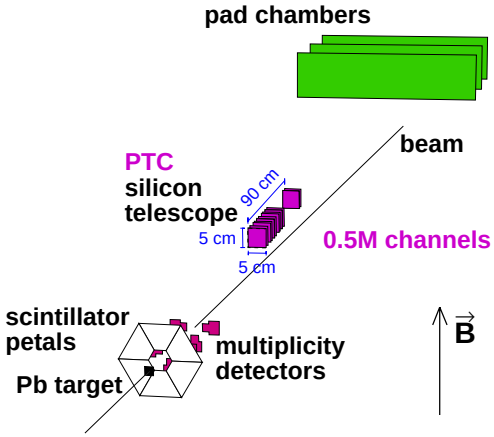

Fig. 2. Sketch of the WA97 set-up

An enhanced production of strange particles in heavy-ion collisions has been observed both at AGS and SPS energies. The enhancement in kaon production at the AGS [6], and perhaps also at the SPS [7,8], can be understood within the hadronic scenario (see e.g. [9]). On the other hand, the data on multi-strange baryon and antibaryon production in Pb–Pb collisions at the SPS, where the Ω enhancement reaches more than one order of magnitude [10,11], are difficult to explain without a QGP production mechanism.

In this paper we shall concentrate on the analysis of transverse mass spectra for strange and multi–strange particles measured by the WA97 experiment. The transverse mass spectra of particles produced in ultrarelativistic nuclear collisions are sensitive to the collision dynamics. The presence of strong radial flow in Pb–Pb collisions at the SPS energy was deduced from the systematics of experimental data on non-strange and singly-strange hadrons, which suggest a linear increase of the inverse slope T with the particle mass m [12,13]. Such a behaviour can be expected in a scenario where a thermal motion is coupled with a transverse collective expansion of the system [14]. The combined analysis of two-pion correlation functions and transverse mass spectra [15] made it possible to separate contributions to the 'apparent temperature' T from a common freeze-out temperature ($\simeq 120$ MeV) and from a transverse flow (with average velocity $\beta_{\perp} \simeq 0.55$).

The WA97 measurement of the Ω inverse slope, presented for the first time in [16] and confirmed later with higher statistics [17], does not fit this picture.

The compilation of data on the m_{T} inverse slopes as a function of the particle mass from the NA44 [12,19,20], NA49 [13,21–23] and WA97 [17,24] experiments is shown in Fig. 1. The measured slope of the Ω (and perhaps also the Ξ) is significantly smaller than expected from the general trend, shown in the figure by the dotted line to guide the eye. This observation favours a scenario in which, in Pb–Pb reactions, multi–strange hadrons freeze out rather early before most of the transverse flow has developed [18].

The published NA44 and NA49 inverse slopes correspond to the most central events ($\simeq 5\%$), while the centrality range of the WA97 data is wider: $\simeq 40\%$ of the most central interactions. Therefore, for a detailed study of the Ω inverse slope anomaly, an analysis of the centrality dependence of the WA97 transverse spectra is essential. This is the main goal of the present work.

In general, knowledge on the centrality dependence of m_{T} spectra is rather scarce. For Pb–Pb collisions, data from the WA98 experiment on π^0 production [25] and from NA45 on negative particles (h^-), pions and 'net proton-like' spectra [26] have been published. Recently the NA49 collaboration has presented the centrality dependence of average p_{T} for pions, kaons and protons [8]. All three experiments reported, at most, a weak centrality dependence.

2 The WA97 experiment

The WA97 experiment is designed to study strange particle production at central rapidity in Pb–Pb collisions as a function of the strangeness content of the particles and of the number of nucleons taking part in the collisions. In order to cope with the high track density in Pb–Pb collisions a powerful tracking device based on silicon pixel detectors has been utilized. This ensures the capability of the experiment to perform an efficient pattern recognition, precise momentum measurement and reliable reconstruction of V^0 decays and multi-strange cascade decays. A current status of the experiment and a review of the recent results are presented in [27].

2.1 Experimental apparatus

The experimental set-up is shown schematically in Fig. 2. The 158 A GeV/c lead beam from the CERN SPS is inci-

dent on a lead target with a thickness corresponding to 1% of an interaction length. Scintillator detectors ('petals') behind the target provided an interaction trigger selecting the most central $\sim 40\%$ of Pb–Pb collisions. Two planes of microstrip multiplicity detectors covering the pseudo-rapidity region $2 \lesssim \eta \lesssim 3$ and $3 \lesssim \eta \lesssim 4$ respectively, provided information for a detailed off-line study of the centrality dependence of particle yields and spectra.

The core of the WA97 set-up is a silicon telescope consisting of 7 planes of the novel pixel detectors [28] which have a pixel size of 75×500 μm^2 and of 10 planes of silicon microstrips with a 50 μm pitch. The telescope has 5×5 cm^2 cross section, containing $\simeq 0.5{\times}10^6$ detecting elements. It acts as a pixel tracking chamber (PTC). This precise tracking device was placed 60 cm downstream from the target slightly above the beam line and inclined by 48 mrad, pointing to the target, in order to accept particles with central rapidity and medium transverse momentum.

The reconstruction of tracks is done in the compact part of the PTC, where 11 planes of silicon detectors are closely packed over a distance of 30 cm. The momentum resolution for fast tracks is improved using lever arm detectors, which consist of additional pixel and microstrip planes and of three MWPC's with a cathode pad readout.

The target and all detectors (except for the pad chambers) are placed inside the homogeneous 1.8 T field of the CERN Omega magnet. The experimental set-up is symmetric with respect to the magnetic bending direction and, therefore, its geometrical acceptance is the same for particles and antiparticles.

2.2 Analysis of strange particle signals

The K^0_S mesons, the Λ, Ξ^- and Ω^- hyperons and their antiparticles were identified by reconstructing their decays into final states containing only charged particles:

$$
\begin{aligned}
\mathrm{K}^0_\mathrm{S} &\rightarrow \pi^+ + \pi^- \\
\Lambda &\rightarrow \mathrm{p} + \pi^- \\
\Xi^- &\rightarrow \Lambda + \pi^- \\
&\quad\ \hookrightarrow \mathrm{p} + \pi^- \\
\Omega^- &\rightarrow \Lambda + \mathrm{K}^- \\
&\quad\ \hookrightarrow \mathrm{p} + \pi^-
\end{aligned}
$$

We have also analysed a reference sample of negatively charged particles (h^-).

The acceptance windows for the particles under study are shown in Fig. 3. Owing to the symmetry of Pb–Pb collisions, the reflection of data with respect to mid-rapidity allows us to extrapolate the particle yields to a region of one rapidity unit centred at mid-rapidity.

The extraction of the strange particle signals is performed using geometric and kinematic constraints. Details of the selection criteria used for the particle identification and for background suppression are discussed in [24,29]. In the reconstructed strange particle mass spectra (see, e.g. [29]) the mass resolution is better than 6 MeV/c^2 (FWHM).

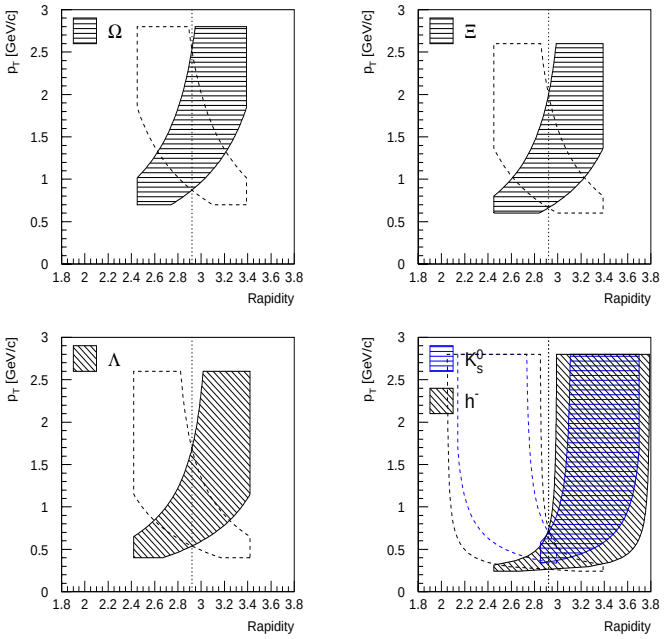

Fig. 3. WA97 acceptance regions for particles produced in Pb–Pb collisions. The windows, reflected with respect to mid-rapidity ($y_{cm} = 2.91$), are drawn with dashed lines

2.3 Data samples and corrections

The results presented in this paper are based on the analysis of a data sample consisting of 110 million Pb–Pb events. The experimental data have to be corrected for geometrical acceptance and for detector and reconstruction efficiency. For the Ξ and Ω data samples (1685 and 203 particles respectively) we have applied an individual weight calculation for each particle. This turned out to be a precise, but very CPU-intensive procedure, not suitable for high statistics samples. Therefore for h^-, K^0_S, Λ and $\overline{\Lambda}$ only a small fraction ($\leq 1\%$) of data were corrected by individual weighting. Statistics in the data samples corrected by event-by-event weighting does not exceed 2000 particles/sample.

For the present study we have also used high statistics samples of h^- and singly-strange particles. To do this corrected m_T spectra have been obtained by applying a method of unfolding the measured distributions (deconvoluted spectra). Statistics for these particles is $\gtrsim 10^5$ events/sample.

Consistency tests demonstrated the full compatibility of m_T spectra from individually weighted and deconvoluted data samples. The main features of both methods used for the data correction, and a comparison between them, are described in the Appendix. As a consistency check, lifetimes of K^0_S, Λ and $\overline{\Lambda}$ particles were calculated by the deconvolution method (see A.4).

In this paper, results of the analysis of both weighted (Ξ^-, $\overline{\Xi}^+$, Ω) and deconvoluted (h^-,K^0_S, Λ, $\overline{\Lambda}$) m_T spectra are presented. Due to the limited statistics the combined data on Ω^- and $\overline{\Omega}^+$were used.

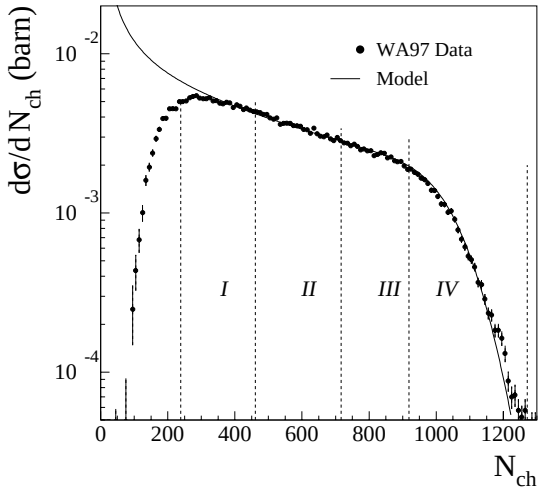

Fig. 4. Wounded nucleon model fit to the multiplicity distribution. The four multiplicity classes, used in the data analysis, are indicated

The data have not been corrected for feed-down. In the geometry of our experiment the feed-down from weak decays is expected to be of minor importance. It is estimated to be less than 5% for Λ and less than 10% for $\overline{\Lambda}$.

2.4 Centrality classes

The WA97 multiplicity detectors allow us to study particle production as a function of collision centrality. As a measure of centrality we use the average number of participants, i.e. nucleons participating in the collision $\langle \mathrm{N}_{part} \rangle$. This is calculated from the measured charged multiplicity in the framework of the wounded nucleon model [30]. The basic assumption of the model is that the average charged particle multiplicity is proportional to $\langle \mathrm{N}_{part} \rangle$. The wounded nucleon model is found to provide a good description of the corrected multiplicity distribution. The details of our approach to the centrality measurement are described in [31].

The result of the fit is presented in Fig. 4. We use four multiplicity classes in the centrality analysis. They are indicated in the figure by dashed lines. The bin widths were chosen so as to contain similar numbers of multi-strange hyperons in each bin before weighting. The data in the first multiplicity bin are corrected for the effect of the centrality trigger. The data samples for multiplicity class IV, corresponding to the most central $\simeq 3.5\%$ of the total inelastic Pb–Pb cross-section, are close in centrality to the NA44 and NA49 data shown in Fig. 1.

3 Results

The double-differential (y, m_{T}) distributions for each particle and for each multiplicity class were fitted using the expression

$$\frac{\mathrm{d}^2 N}{\mathrm{d}m_{\mathrm{T}}\,\mathrm{d}y} = f(y)\, m_{\mathrm{T}}\, \exp\left(-\frac{m_{\mathrm{T}}}{T}\right) \qquad (1)$$

Table 1. Inverse m_{T} slope parameters T for Pb–Pb interactions.

Particle	Inverse slope T (MeV)
h^-	197 ± 2
$\mathrm{K}^0_{\mathrm{S}}$	230 ± 2
Λ	289 ± 3
$\overline{\Lambda}$	287 ± 4
Ξ^-	286 ± 9
$\overline{\Xi}^+$	284 ± 17
$\Omega^- + \overline{\Omega}^+$	251 ± 19

where $m_{\mathrm{T}} = \sqrt{m^2 + p_T^2}$ is the transverse mass, assuming the rapidity distribution to be flat in our acceptance region ($f(y) = const.$) and leaving the inverse slope T as a free parameter of fit. The fit was performed using the method of maximum likelihood for the weighted spectra and the minimum χ^2 for the deconvoluted spectra. Preliminary data on the rapidity distributions of the singly-strange particles (deconvoluted spectra) support our assumption on the flatness of the rapidity distribution near mid-rapidity [32].

3.1 Transverse mass spectra

The inverse slope parameters T of transverse mass spectra for h^- and strange particles measured in Pb–Pb collisions, in the full acceptance and centrality range accessible to the experiment, are summarised in Table 1.

For h^-, $\mathrm{K}^0_{\mathrm{S}}$, Λ and $\overline{\Lambda}$ the slopes were determined from high statistics data samples by fitting expression (1) to the deconvoluted (y, m_{T}) spectra. For negative hadrons, considered as pions, the fitting was performed in the range $0.4 < m_{\mathrm{T}} < 0.9$ GeV/c^2. It is worth emphasizing that new precise data on $\mathrm{K}^0_{\mathrm{S}}$, Λ and $\overline{\Lambda}$ inverse slopes are in good agreement with our previous results [24]. For completeness we present in the table also our recent results on multi-strange hyperons [24].

As one can see from Fig. 1, the inverse slope values for singly-strange particles follow the general trend (linear increase of T with the particle mass), considered as evidence for collective radial flow [12,14,33], but the slopes for multi-strange particles do not.

The inverse m_{T} slopes for Λ and Ξ are very similar, while a decrease in T is observed for the heavier Ω hyperon. As mentioned in Sect. 1, this behaviour can be understood in terms of a scenario where the transverse flow develops late, after most of the multi-strange particles have already frozen out [18].

3.2 Centrality dependence of inverse slopes

To investigate the observed Ω inverse slope anomaly in detail we have performed a centrality dependence analysis of

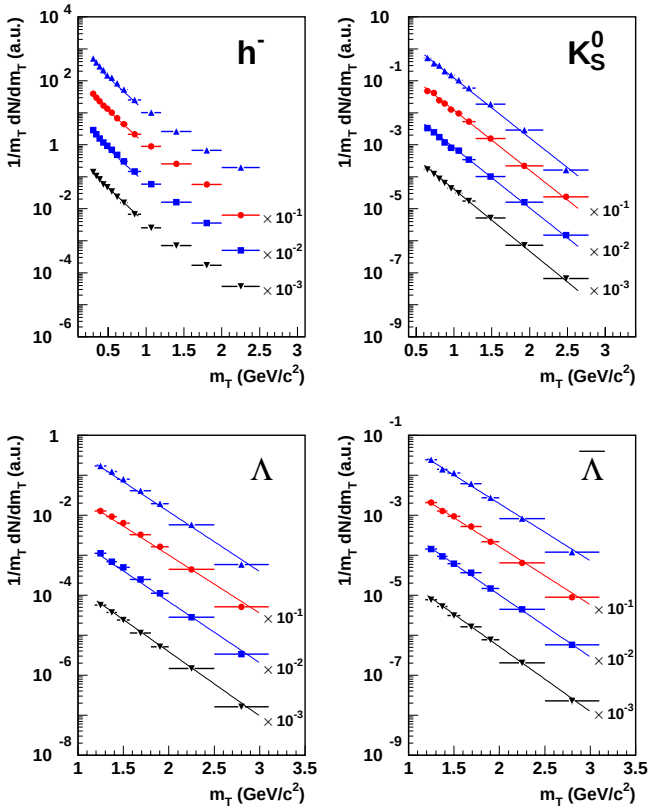

Fig. 5. Transverse mass spectra of h^-, K^0_S, Λ and $\overline{\Lambda}$ shown separately for the four centrality classes. Data for the most central events are shown on the top, data for the most peripheral events (divided by 10^3) in the bottom of each picture

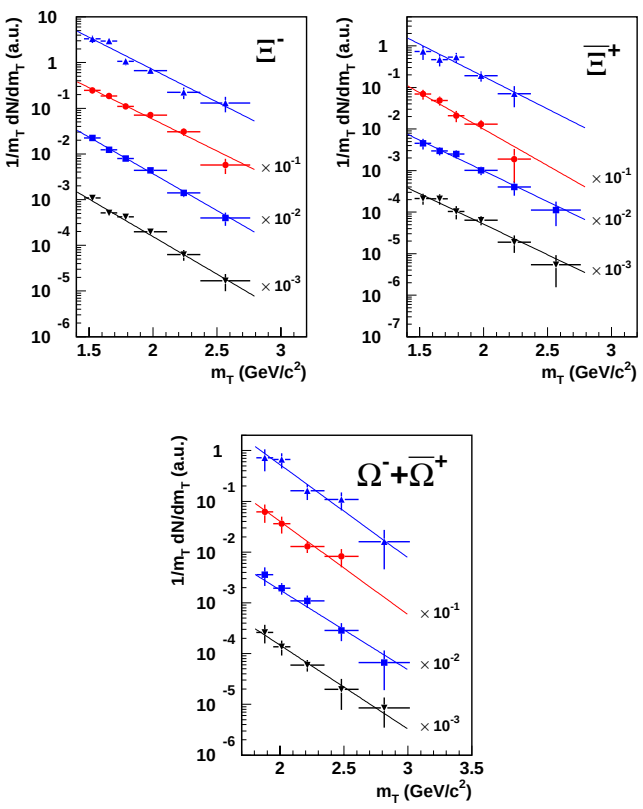

Fig. 6. Transverse mass spectra of Ξ^-, $\overline{\Xi}^+$ and Ω shown separately for the four centrality classes. Data for the most central events are shown on the top, data for the most peripheral events (divided by 10^3) in the bottom of each picture

the $m_{\rm T}$-spectra. We have fitted the corrected experimental data by formula (1) separately for each of the four multiplicity bins indicated in Fig. 4.

For h^-, K^0_S, Λ and $\overline{\Lambda}$ the deconvoluted $m_{\rm T}$ spectra, based on high statistics data samples, were used for this analysis. They are presented for different multiplicity bins in Fig. 5.

For Ξ^-, $\overline{\Xi}^+$ and Ω we use all available data, corrected by the individual weighting method. The $m_{\rm T}$ spectra for multi-strange particles are shown in Fig. 6 separately for each multiplicity class.

The lines, superimposed on the $m_{\rm T}$ spectra in Figs. 5 and 6, are the exponential functions with T values resulting from fits.

The transverse mass spectra for K^0_S, Λ, $\overline{\Lambda}$, Ξ^-, $\overline{\Xi}^+$and Ω are described satisfactorily by an exponential function in all the accessible $m_{\rm T}$ regions (up to $\simeq 3$ GeV/c^2).

As can be seen in Fig. 5, the $m_{\rm T}$ distribution for negative hadrons, dominated by pions, exhibits a more complicated behaviour. The substantial contribution of pions from resonance decays to the low transverse mass region results in a steepening of the $m_{\rm T}$ spectrum. In order to exclude the region where slow pions from resonance decays are mostly concentrated, we restricted our centrality analysis of h^- to the intermediate transverse mass region ($0.4 < m_{\rm T} < 0.9$ GeV/c^2), where a fit by a single exponential function is adequate.

For h^- we have also performed fits for the higher transverse mass region ($0.8 < m_{\rm T} < 2.0$ GeV/c^2), where the admixture of pions from resonance decays is negligible. In this region the inverse slopes T are, for all centrality bins, close to 240 MeV, in agreement with the recent NA45 results [26]. The similarity of this slope parameter with that for kaons is consistent with the theoretical expectation that for a thermalized expanding fireball in the relativistic region ($p_{\rm T} \gg m$) all particles should have the same slope [14].

The dependence of the inverse slopes T on the number of participants N_{part}, resulting from the fits to $m_{\rm T}$ spectra for different centrality bins, is shown in Fig. 7.

The h^- and K^0_S slopes appear to be constant in the $N_{part} > 100$ range. Values of T for Λ, $\overline{\Lambda}$, and probably also for Ξ^-, exhibit a slow but steady rise, up to 15% in the centrality range under study. The inverse slopes of $\overline{\Xi}^+$and Ω spectra do not exhibit a significant centrality dependence. This indicates that the Ω inverse slope anomaly (see Fig. 1) is present in all our centrality range.

The mass dependence of inverse slopes, measured for the most central bin ($\langle N_{part} \rangle \simeq 350$) is shown in Fig. 8.

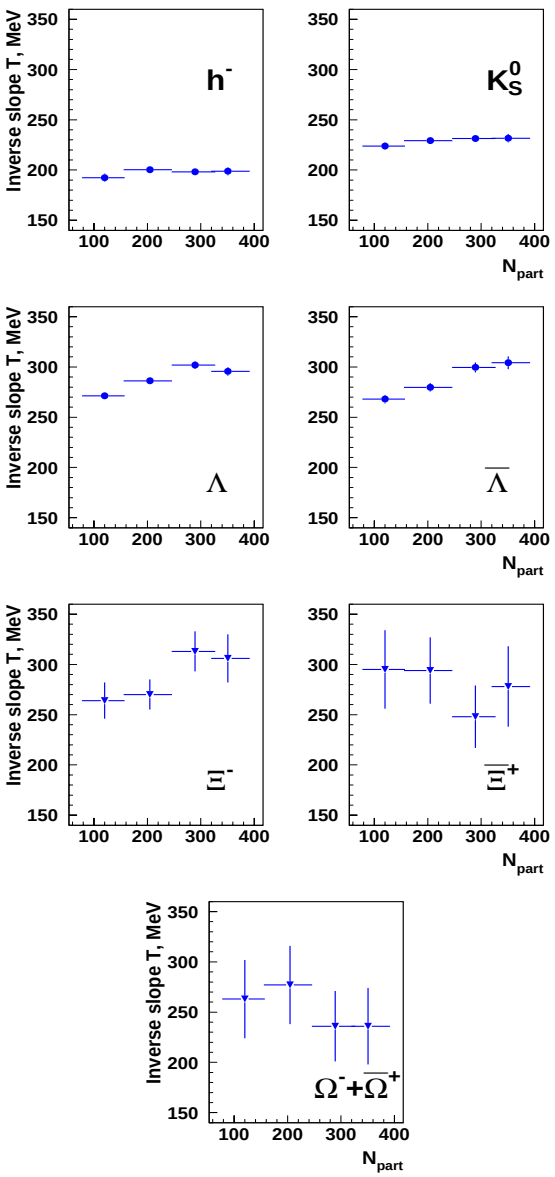

Fig. 7. Dependence of m_{T} spectra inverse slopes T on the centrality of collision

The dotted line indicating the general trend is the same as in Fig. 1. The deviation of the Ω slope from the linear mass dependence is clearly seen for our most central Pb–Pb events, which are close in centrality to the NA44 and NA49 data plotted in Fig. 1.

4 Conclusions

We have analysed the transverse mass spectra of negative hadrons and strange particles produced in Pb–Pb collisions at 158 A GeV/c.

The centrality dependence of the inverse slopes T for all particles under study is found to be weak and does not exceed 15% in the centrality range $\mathrm{N}_{part} > 100$.

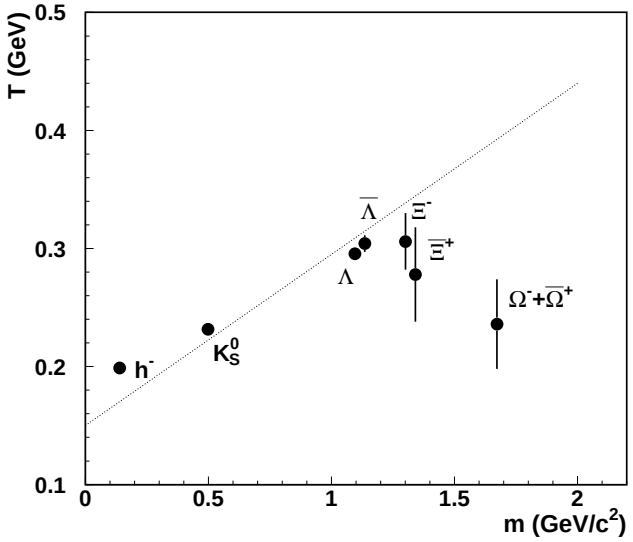

Fig. 8. Mass dependence of inverse slopes for the most central Pb–Pb events measured in the WA97 experiment

The measured inverse m_{T} slopes T of singly-strange particles are in good agreement with the recently observed linear increase of T with the particle mass. However, the Ω inverse slope deviates significantly from this linear dependence, suggesting that, in Pb–Pb collisions, multi-strange baryons decouple early from the hot and dense expanding system [18]. This deviation is seen for Pb–Pb collisions in all our centrality range.

Acknowledgements. We are grateful to U. Heinz for fruitful discussions and useful comments.

Appendix A: Data correction methods

Two methods have been used to extract the experimental distribution of measured particles:
a) individual weighting of each reconstructed particle,
b) deconvolution of measured spectra.
Here we describe the main points of both methods.

The objective is to measure the distribution $f(x)$ of the physical variable x. The variable x can be multidimensional, e.g. in the case of the two body decay of a particle (for example Λ) there are six components of x:

$$x = \{y, m_{\mathrm{T}}, \Phi, \tau, \phi, \theta\}$$

where y is the rapidity, m_{T} is the transverse mass and Φ is the azimuthal angle of the particle in the laboratory, τ is its lifetime and ϕ and θ are angles determining the direction of the decay products in the rest system of the decaying particle. Let us divide these six variables into two groups:

- variables for which we want to find the distribution f (denote these as s'). In the analysis presented in this paper we are interested in rapidity and transverse mass, and therefore $s' = \{y, m_{\mathrm{T}}\}$;

- variables for which we assume the distribution f to be known and we integrate over them. Let us denote them $t' = \{\Phi, \tau, \phi, \theta\}$.

In the process of measurement, the distribution $f(s', t')$ is distorted due to the effects of the limited acceptance, detector and reconstruction efficiency, as well as the finite resolution of the detector. Instead of s' the quantity s is measured with the distribution $g(s)$. The relation between the measured distribution g and the distribution f is:

$$g(s) = \int A(s, s', t, t') f(s', t') ds' dt dt' \ . \tag{2}$$

The function A describes the response of the detector including acceptance, efficiency and resolution. The function A is not known explicitly. It can be determined by a Monte-Carlo (MC) simulation of the detector.

We shall assume that the distribution f factorizes:

$$f(s', t') = u(s')v(t') \ .$$

Moreover, all variables included in t' are assumed to be independent.

A.1 Weighting method

In this method the approximation of the resolution function A

$$A(s, s', t, t') = A(s, t, t')\delta(s - s')$$

is used. The approximation is justified by the fact that the resolution of our detector is much better than the magnitude of the parameter we want to determine. (The inverse slopes of transverse mass distributions are in the range 200 - 300 MeV for the transverse momenta in the range 300 MeV/c to 3 GeV/c and the resolution is of the order of 1%). After this approximation equation (2) is reduced to

$$g(s) = u(s) \int A(s, t, t')v(t') dt dt'$$

and the quantity

$$w(s) = u(s)/g(s) = \frac{1}{\int A(s, t, t')v(t') dt dt'}$$

is the weight for the particle with the kinematical characteristics s (in our case s represents the rapidity y and transverse mass m_{T}).

The weight for each particle is calculated by a MC procedure with the following main steps:

(1) For each observed particle a sample of MC particles with the measured values of y and m_{T} is generated. They are propagated, using the standard simulation tool GEANT [34], through the experimental set-up.
(2) To simulate background conditions, the hits corresponding to each MC particle and their decay products are embedded in a real event with similar characteristics to the one with the observed particle.
(3) The mixed events are processed with the same chain of programs (track finding, signal reconstruction and selection) as the real data.

The resulting weight is the number of MC particles generated divided by the number of MC particles succesfully reconstructed.

A.2 Deconvolution method

Here we follow the general principles of unfolding methods (see e.g. review [35]). We convert the equation (2) to a discrete form using the matrix representation:

$$g = Af \tag{3}$$

where $g = [g_1, g_2, \ldots, g_N]$ is the histogram of measured data, $f = [f_1, f_2, \ldots, f_N]$ is the histogram of deconvoluted data and

$$A = \begin{pmatrix} A_{11} & A_{12} & \ldots & A_{1N} \\ A_{21} & A_{22} & \ldots & A_{2N} \\ \vdots & \vdots & \ddots & \vdots \\ A_{N1} & A_{N2} & \ldots & A_{NN} \end{pmatrix}$$

is the response matrix. The covariance matrix of g is diagonal:

$$V_0 = \begin{pmatrix} g_1 & 0 & 0 & \ldots & 0 \\ 0 & g_2 & 0 & \ldots & 0 \\ 0 & 0 & g_3 & \ldots & 0 \\ \vdots & \vdots & \vdots & \ddots & \vdots \\ 0 & 0 & \ldots & 0 & g_N \end{pmatrix} .$$

The vector f can be obtained by inversion of matrix equation (3):

$$f = A^{-1}g.$$

The covariance matrix of f is then:

$$V_f = A^{-1}V_0 A^{T-1} \ .$$

The matrix A has to be determined. This calculation is based on the detailed simulation of the WA97 detector response.

Using on the right side of equation (3) the vector $v = [1, 0, \ldots, 0]$ we get

$$Av = [A_{11}, A_{21}, \ldots, A_{N1}] \tag{4}$$

which is the first column of matrix A . Using an input vector with only one non-zero element at the $i - th$ place gives us the $i - th$ column of matrix A.

The determination of the matrix A is technically similar to the weight calculation, and the same software chain can be used for the following tasks:

(1) The MC events are generated with distribution f_{MC}. (To optimize the computing efficiency the MC event distribution is chosen to be as close as possible to the expected true distribution f.)

(2) To simulate background tracks and electronic noise the MC events are embedded in the real events, taking into account the detector efficiency.
(3) The mixed events are processed with the same chain of reconstruction and analysis programs as the real data.
(4) The matrix A according to equation (4) is produced.
(5) The equation (3) is solved.

We finish this description with two comments on the application of the deconvolution method.

(1) The statistical error of any quantity calculated from vector f is fully determined by the covariance matrix V_f. Due to the finite sample of MC events from which the response matrix A was calculated an additional error is present. This error was estimated by simulation. For the data presented in this paper this error was of the same order as the statistical one. The resulting errors were calculated assuming that the statistical error and uncertainty in the response matrix are independent.
(2) It is discussed in the literature (see e.g. [35,36]) that the direct inversion of equation (3) might be unstable and could lead to oscillations. If this is the case, methods of statistical regularisation can be applied. However, for the binning of data used in this paper the matrix A was dominantly 3-diagonal. The inversion procedure turned out to be stable and no regularisation was required.

A.3 Comparison of methods

We have compared the values of the inverse slope parameters T obtained from the fits to the weighted and deconvoluted data for h^-, K^0_S, Λ and $\overline{\Lambda}$ (where the samples of both data types are available).

In both cases the formula (1) was fitted to the data. For the sample of weighted particles the maximum likelihood method was used and a χ^2 fit to the two dimensional histogram of unfolded data was performed. The results are presented in Fig. 9 and show that the two methods are compatible.

A.4 K^0_S, Λ and $\bar{\Lambda}$ lifetimes

As a consistency check of the unfolding procedure the lifetimes of K^0_S, Λ, $\overline{\Lambda}$ particles were determined. A two-dimensional deconvolution in the variables τ and m_T was performed. The rapidity was restricted to a narrow window $2.9 < y_{lab} < 3.3$ for Λ and $\overline{\Lambda}$ particles and to $2.8 < y_{lab} < 3.4$ for K^0_S. The χ^2 fit with the function

$$\frac{\mathrm{d}^2N}{\mathrm{d}m_T\,\mathrm{d}\tau} \propto m_T \exp\left(-\frac{m_T}{T}\right)\exp\left(-\frac{\tau}{\tau_{part}}\right)$$

was performed. τ_{part} is the lifetime of a given particle (K^0_S, Λ, $\overline{\Lambda}$). The τ projections of (τ, m_T) deconvoluted spectra, corrected for the m_T acceptance, are presented in Fig. 10.

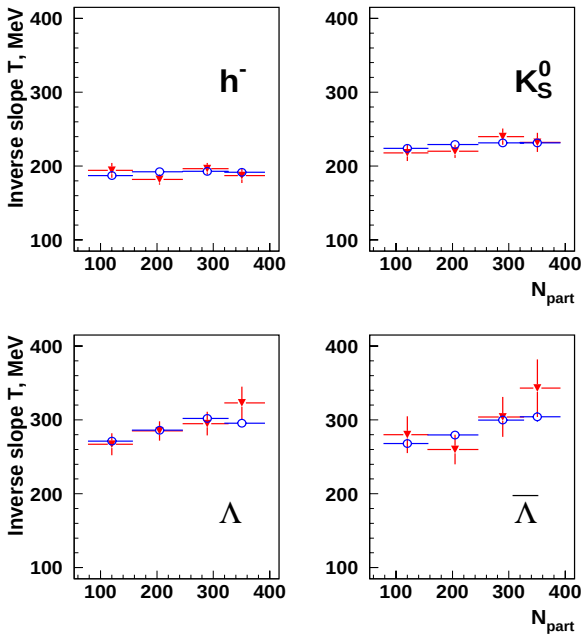

Fig. 9. Comparison of the m_T spectra inverse slopes T obtained by the weighting (solid triangles) and deconvolution (empty circles) methods

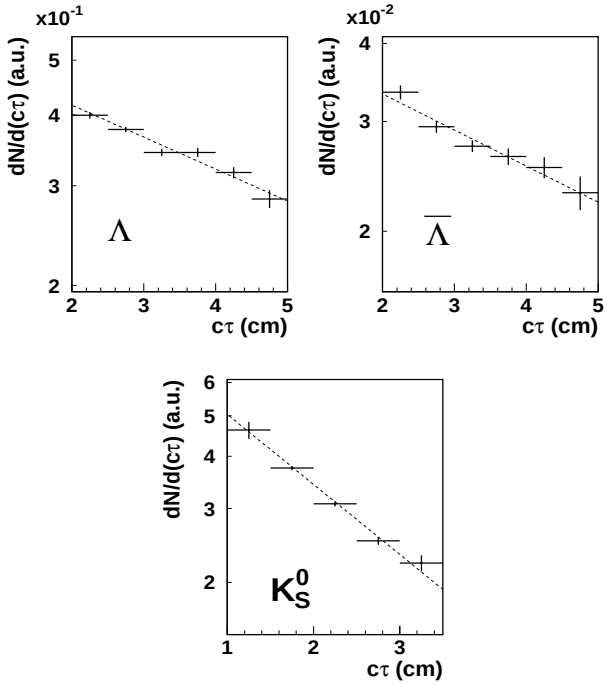

Fig. 10. The distribution of $c\tau$ for Λ,$\bar{\Lambda}$ and K^0_S

The superimposed lines represent exponential functions with the fitted lifetimes. The corresponding $c\tau_{part}$ values are:

$$c\tau_{K^0_S} = 2.6 \pm 0.1\ cm$$
$$c\tau_{\Lambda} = 7.6 \pm 0.5\ cm$$
$$c\tau_{\overline{\Lambda}} = 7.5 \pm 0.9\ cm.$$

A good agreement of these results with the PDG values is obtained, showing that our unfolding procedure is satisfactory.

References

1. J.W. Harris and B. Müller, Annu. Rev. Nucl. Part. Sci. **46** (1996) 71.
2. S.A. Bass, M. Gyulassy, H. Stöcker and W. Greiner, J. Phys. G: Nucl. Part. Phys. **25** (1999) R1.
3. J. Rafelski and B. Müller, Phys. Rev. Lett. **48** (1982) 1066; Phys. Rev. Lett. **56** (1986) 2334.
4. P. Koch, B. Müller and J. Rafelski, Phys. Rep. **142** (1986) 167.
5. J. Rafelski. Phys. Lett. B **262** (1991) 333.
6. L. Ahle *et al.* (E802 coll.), nucl-ex/9903009.
7. I. Bearden *et al.*, nucl-ex/9907013.
8. F. Sikler *et al.*, Nucl. Phys. A **661** (1999) 45c.
9. J.C. Dunlop and C.A. Ogilvie. nucl-th/9911015.
10. E. Andersen *et al.*, Phys. Lett. B **433** (1998) 209.
11. E. Andersen *et al.*, Phys. Lett. B **449** (1999) 401.
12. I.G. Bearden *et al.*, Phys. Rev. Lett. **78** (1997) 2080.
13. T. Alber *et al.*, J. Phys. G: Nucl. Part. Phys. **23** (1997) 1817.
14. K.S. Lee, U. Heinz and E. Schnedermann. Z. Phys. C **48** (1990) 525.
15. H. Appelshäuser *et al.*, Eur. Phys. J. C **2** (1998) 661.
16. I. Králik for the WA97 collaboration, Nucl. Phys. A **638** (1998) 115c.
17. R.Caliandro for the WA97 collaboration, J. Phys. G: Nucl. Part. Phys. **25** (1999) 171.
18. H. van Hecke, H. Sorge and Nu Xu, Phys. Rev. Lett. **81** (1998) 5764.
19. I.G. Bearden *et al.*, Nucl. Phys. A **638** (1998) 419c.
20. I.G. Bearden *et al.*, Nucl. Phys. A **638** (1998) 103c.
21. S.V. Afanasiev *et al.*, Nucl. Phys. A **610** (1996) 188c.
22. H. Appelshäuser *et al.*, Nucl. Phys. A **638** (1998) 91c.
23. H. Appelshäuser *et al.*, Phys. Lett. B **444** (1988) 523.
24. R. Lietava for the WA97 collaboration, J. Phys. G: Nucl. Part. Phys. **25** (1999) 181.
25. M.M. Aggarwal *et al.*, Phys. Rev. Lett. **81** (1998) 4087.
26. F. Ceretto for the CERES collaboration, Nucl. Phys. A **638** (1998) 467c.
27. F. Antinori for the WA97 collaboration, Nucl. Phys. A **661** (1999) 130c.
28. E.H.M. Heijne *et al.*, Nucl. Instrum. Methods A **349** (1994) 138; F. Antinori *et al.*, Nucl. Instrum. Methods A **360** (1995) 91.
29. L. Šándor for the WA97 collaboration, Nucl. Phys. B (Proc. Suppl.) **71** (1999) 270.
30. A. Bialas, M. Bleszynski and W.Czyz. Nucl. Phys. B **111** (1976) 461.
31. F. Antinori *et al.* : Determination of the number of wounded nucleons in Pb+Pb collisions at 158 A GeV/c. CERN-EP-2000-002; submitted to Eur. Phys. J. C.
32. D. Evans for the WA97 collaboration, Proc. of the XVth Particles and Nuclei International Conference (PANIC'99), Uppsala, Sweden, June 1999 (*to be published*)
33. S. Esumi, S. Chapman, H. van Hecke and N. Xu. Phys. Rev. C **55** (1997) R2163.
34. GEANT, CERN Program Library, W5013
35. V. Blobel: Unfolding methods in high-energy physics. Proceedings of the 1984 CERN school of computing, CERN 85-09 (1985) p. 88-127.
36. A.N. Tikhonov, V.Ya. Arsenin. Methods of ill-posed problems solving. Nauka, Moscow, 1979 (in russian).